Contribution of Extragalactic Infrared Sources to CMB Foreground Anisotropy

Eric Gawiser and George F. Smoot

Department of Physics and Lawrence Berkeley National Laboratory, University of California, Berkeley, Berkeley, CA 94720

ABSTRACT

We estimate the level of confusion to Cosmic Microwave Background (CMB) anisotropy measurements caused by extragalactic infrared sources. CMB anisotropy observations at high resolution and high frequencies are especially sensitive to this foreground. We use data from the COBE satellite to generate a Galactic emission spectrum covering mm and sub-mm wavelengths. Using this spectrum as a template, we predict the microwave emission of the 5319 brightest infrared galaxies seen by IRAS. We simulate skymaps of extragalactic infrared sources over the relevant range of frequencies (30-900 GHz) and instrument resolutions ($10' - 10°$ FWHM). Analysis of the temperature anisotropy of these skymaps shows that a reasonable observational window is available for CMB anisotropy measurements.

Subject headings: cosmic microwave background – infrared: galaxies – galaxies: spiral

1.   Introduction

The COBE detection of large-angular scale Cosmic Microwave Background anisotropy (Smoot et al. 1992) has generated interest in measuring CMB anisotropy on all angular scales with the goal of determining cosmological parameters. Current anisotropy observations look at sub-degree angular scales which correspond to observable structures in the present universe. Improved instrumentation and the MAP (Microwave Anisotropy Probe) and Max Planck Surveyor (formerly COBRAS/SAMBA) satellite missions focus attention on angular scales between one-half and one-sixth of a degree.

Due to its large beam size, COBE was basically unaffected by extragalactic foreground sources (Banday et al. 1996, Kogut et al. 1994). Because the antenna temperature contribution of a point source increases with the inverse of the solid angle of the beam, observations at higher angular resolution are more sensitive to extragalactic foregrounds, including radio sources, the Sunyaev-Zel'dovich effect from galaxy clusters, and the infrared-bright galaxies examined here.

Previous work in this area (Toffolatti et al. 1994, Franceschini et al. 1989, Wang 1991) used galactic evolution models with specific assumptions about dust temperatures to predict the level of extragalactic foreground. We choose instead a phenomenological approach using the infrared-bright galaxies detected by the Infrared Astronomical Satellite (IRAS) and the Galactic emission detected by the COBE (Cosmic Background Explorer) satellite. Section 3 compares our results with those from galaxy-evolution models.

The FIRAS (Far-Infrared Absolute Spectrophotometer) instrument of COBE gives evidence for the existence of Cold (< 15K) Dust in the Galactic plane (Reach et al. 1995). If the Milky Way has Cold Dust, then it is likely present in other dusty spirals, which comprise the majority of bright extragalactic infrared sources. Some observations (Chini et al. 1995, Block et al. 1994, Devereux & Young 1992) indicate the presence of Cold

Dust in other galaxies. Neither galactic evolution models nor pre-FIRAS observations (see Eales et al. 1989) were able to set tight constraints on emission from Cold Dust, but the FIRAS observations do. Emission from dust close in temperature to the 2.73 K background radiation is difficult to separate from real CMB anisotropies. If Cold Dust is typically accompanied by Warm Dust in spiral galaxies, we can use the FIRAS information about the total dust emission of the Galaxy to overcome this spectral similarity.

2. Extragalactic Infrared Sources

The far-infrared discrete sources detected by IRAS are typically inactive spiral galaxies, although some are quasars, starburst galaxies, and Seyfert galaxies. The IRAS 1.2 Jy catalog (Fisher et al. 1995) provides flux measurements of 5319 galaxies at 12, 25, 60, and 100 μm, where interstellar dust emission is dominant. We compared the locations of these galaxies with those of a thousand of the brightest radio sources, and only 7 possible coincidences resulted. This lack of coincidence shows that radio-loud galaxies can be treated separately. The IRAS sources are roughly isotropic in distribution, except for a clear pattern of the Supergalactic Plane. To reduce the possibility of residual galactic contamination, we use a skymap in our analysis that covers galactic latitudes $|b| > 30°$. This map contains contributions from 2979 galaxies for a 0°.5 beam.

The nature of dust in spiral galaxies is still an open question. It seems likely that there is dust at widely varying temperatures and possibly with different emissivities (Rowan-Robinson 1992, Franceschini & Andreani 1995). Attempts to fit observational data have yielded a variety of results; it is unclear if far-infrared luminous dust is well described by a one-component or a two-component model, and the emissivity power-law index is only known to be between 1 and 2. We avoid specifying the nature of this dust by using the observed Galactic far-infrared emission spectrum as a template for IRAS galaxies. To

check the accuracy of this template, we fit a two-component dust model to IRAS galaxies and to the integrated 12, 25, 60, and 100 μm fluxes of the Milky Way measured by the DIRBE (Diffuse Infrared Background Experiment) instrument of COBE. This produces similar results for the Warm (15-40 K) Dust component to which IRAS and DIRBE are most sensitive; for an emissivity power-law index of 1.5, DIRBE gives a Warm Dust temperature of 28K for the Milky Way, while the 425 IRAS galaxies with highest-quality flux measurements are collectively fit to a Warm Dust temperature of 33K. This Warm Dust accounts for the majority of the far-infrared emission of spiral galaxies.

There is, however, observational evidence that the far-infrared emission of inactive spirals is dominated by dust slightly colder than 20K (Neininger & Guelin 1996, Chini & Krugel 1993). Fitting the FIRAS spectrum of the Milky Way also leads to a Warm Dust temperature close to 20K. These fits appear to conflict with the temperatures found above using IRAS and DIRBE fluxes at $\lambda \leq 100\mu$m. Using 60, 100, 140, and 240 μm DIRBE fluxes, however, indicates a Warm Dust temperature for the Galaxy of 24K. This shows that temperature fits to data on one side of the peak of the assumed blackbody spectrum can be inaccurate. Figure 1 shows that the spectra of the Milky Way found by DIRBE and FIRAS are indeed compatible. It may be an oversimplification to represent the Warm Dust in a galaxy by a single temperature.

We recognize that not all IRAS galaxies have exactly the same far-IR spectrum as the Milky Way. Active galaxies are warmer, with an average Warm Dust temperature of 33K (for emissivity index 2, Chini et al. 1995). However, the cirrus emission which dominates Galactic dust is consistent with the emission from the majority of inactive spirals (Andreani & Franceschini 1996, Pearson & Rowan-Robinson 1996). Some observations indicate that our Galaxy is slightly warmer than the average inactive spiral (Chini et al. 1995). None of these observations includes enough frequencies to provide a template microwave

emission spectrum, and their results range by a factor of 3 depending on the choice of beam corrections (Franceschini & Andreani 1995). The Milky Way is a good middle-of-the-road choice for a microwave template spectrum; the DIRBE and IRAS dust temperature fits given above agree rather well.

After removing Galactic emission lines (as in Reach et al. 1995), we fit a dust model to the FIRAS dust spectrum. The CO 1-0 emission line at 115 GHz is not clearly detected by FIRAS but could be responsible for increased emission at that frequency. It is possible to vary the parameters of the dust model significantly and still have an acceptable fit, so we refrain from giving any physical importance to the parameters of the fit. We add synchrotron and free-free components with microwave-range spectral indices of -1.0 and -0.15, respectively, so that these sources of microwave emission match COBE DMR (Differential Microwave Radiometer) observations below 100 GHz (Kogut et al. 1996, Reach et al. 1995, Bennett et al. 1992). Free-free emission is stronger than dust beyond the low-frequency end of the FIRAS spectrum.

We combine data from DIRBE, FIRAS, and DMR to form the broad Galactic spectrum shown in Figure 1. Each IRAS 1.2 Jy source is fit to the DIRBE end of the spectrum and extrapolated to the desired frequency using this template. In fitting each IRAS galaxy to the DIRBE fluxes of the Milky Way, we give more weight to the 60 and 100 μm fluxes, which are most sensitive to Warm Dust, than to the 12 and 25 μm fluxes, which are also sensitive to Hot (100-300 K) Dust. The 1.2 Jy catalog gives redshifts for these galaxies. Most have $z < 0.05$ and all have $z < 0.3$. We take these redshifts into account while fitting and extrapolating.

It would be advantageous to fit each type of galaxy to a specialized far-IR to microwave spectrum, but no other trustworthy template spectrum is currently available, so we use the Galactic far-infrared emission spectrum for all sources. The Galactic spectrum agrees

well with observed correlations between radio and IR fluxes of IRAS galaxies (Condon & Broderick 1991, Crawford et al. 1995). Our template spectrum is consistent with detections and upper limits for bright infrared galaxies from DIRBE (Odenwald, Newmark & Smoot 1995). This is helpful because DIRBE used 140 and 240 μm channels, which IRAS lacks, allowing it to probe much cooler dust temperatures than IRAS. DIRBE rules out the possibility of extremely bright sources occurring in the 2% of the high Galactic latitude sky not surveyed by IRAS and sees no evidence for sources whose emission comes predominantly from Cold Dust.

3. Results

We use the Galactic far-infrared emission spectrum to predict the microwave flux of each IRAS galaxy in Jy (1 Jy = $10^{-26}W/m^2$/Hz). To convert from flux S to antenna temperature T_A, we use

$$T_A = S\frac{\lambda^2}{2k_B\Omega} \ ,\tag{1}$$

where k_B is Boltzmann's constant, λ is the wavelength, and Ω is the effective beam size of the observing instrument. Antenna temperature is related to thermodynamic temperature by

$$T_A = \frac{x}{e^x - 1} \ T,\tag{2}$$

defining $x \equiv h\nu/kT$. Small fluctuations in antenna temperature can be converted to effective thermodynamic temperature fluctuations using

$$\frac{dT_A}{dT} = \frac{x^2 e^x}{(e^x - 1)^2} \quad .$$ (3)

Analysis of source counts indicates that the 1.2 Jy sample is complete down to an extrapolated flux of 3 mJy at 100 GHz. We divide the sources logarithmically into groups of similar flux and find a gradual decrease in anisotropy as flux decreases, indicating that dimmer sources will not generate significant anisotropy. Toffolatti et al. (1995) found a negligible contribution from non-Poissonian fluctuations. Poissonian fluctuations should be dominated by those sources prevalent enough to have roughly one source per pixel. For an instrument with a resolution of $10'$ to have one source per beam, we must look at sources with $z \simeq 0.24$. Assuming $(1 + z)^3$ luminosity evolution and including k-correction (see Pearson & Rowan-Robinson 1996, Beichman & Helou 1991), these sources will generate a temperature anisotropy only 2% of that caused by IRAS 1.2 Jy galaxies. High redshift galaxies should produce a significant isotropic cosmic infrared background (Hauser 1995) but should be too distant to produce significant foreground anisotropy. We therefore expect the anisotropy generated by sources too dim to make the 1.2 Jy catalog to be a small part of the total anisotropy; the brightest sources are generating most of the fluctuations.

To simulate observations, we convolve all sources on pixelized skymaps (2X oversampled) of resolution varying from $10'$ to $10°$. The resulting maps, covering a range of frequencies from 30 to 900 GHz, are analyzed to determine the expected contribution of IRAS galaxies to foreground confusion of CMB temperature anisotropy. The information contained in these skymaps can be used to choose regions of the sky in which to observe (Smoot et al. 1995). The contour plot in Figure 2 shows the rms thermodynamic temperature anisotropy produced by extragalactic infrared sources over the full range of frequencies and instrument resolution. The minimum value of $\frac{\Delta T}{T}$ is 1.3×10^{-8} at large FWHM and medium frequency and the maximum value is 0.092 at small FWHM and

high frequency. For frequency in GHz and FWHM in degrees, our results for temperature anisotropy are fit to within 10% by

$$\log_{10}\frac{\Delta T}{T} = 2.0(\log_{10}\nu)^3 - 8.6(\log_{10}\nu)^2 + 10.3\log_{10}\nu - 0.98\log_{10}(FWHM) - 9.2 \qquad (4)$$

The inverse linear relationship between anisotropy and FWHM results from the combined effects of beam convolving and map pixelization. Anisotropy from extragalactic infrared sources dominates expected CMB anisotropy at frequencies above 500 GHz. This makes effective foreground discrimination possible for instruments with a frequency range sufficiently wide to detect the extragalactic infrared foreground directly.

Figure 3 shows a summary of our results for several benchmark instrument resolutions. The dashed lines represent the results of subtracting pixels where the fluctuations from extragalactic infrared sources are five times times greater than the quadrature sum of the rms CMB anisotropy and the expected instrument noise for the Max Planck Surveyor at that frequency (Tegmark & Efstathiou 1995). These 5σ pixels can be assumed to contain bright point sources. Our results agree closely with those of Toffolatti et al. (1995) for their model of moderate cosmological evolution of all galaxies. Our predictions for anisotropy are lower by about a factor of three than those of Franceschini et al. (1989), who assume strong evolution of the brightest IR sources and include early galaxies with heavy starburst activity. Wang (1991) ignores the possibility of cold dust and uses galaxy evolution models to predict anisotropy levels somewhat lower than those found with our phenomenological approach.

The 5σ subtraction has a significant effect for small FWHM at frequencies below 500 GHz. The maximum effect is to subtract 0.002% of the pixels, leading to a factor of 5 reduction in foreground temperature anisotropy. This is further evidence that temperature

anisotropy from extragalactic infrared sources is dominated by the brightest sources. The bright sources are a mixture of Local Group galaxies and more distant infrared-luminous galaxies such as starburst galaxies. Optimal subtraction of the extragalactic infrared foreground requires the contribution from each bright source to be predicted accurately.

4. Discussion

Our usage of the Galactic far-infrared emission spectrum as a template causes systematic errors on a galaxy-by-galaxy basis. It is easy to place constraints on our results; if all galaxies had only 33K dust as is typical for active galaxies, the resulting anisotropy would be a factor of 100 lower. This is highly unlikely, because we know that most IRAS galaxies are inactive spirals, and galaxies with colder dust will dominate the anisotropy at mm-wavelengths because of the selection effect favoring sources with flatter spectra. A robust upper limit on microwave anisotropy from infrared galaxies can be set by assuming that our IRAS 1.2 Jy galaxies cause the full cosmological far-infrared background (for which Puget et al. 1996 claims a detection and Mather et al. 1994 gives an upper limit). In this case we have underestimated the anisotropy by a factor of 100, but no predictions of the IR background expect these nearby galaxies to produce more than a few percent of it. A more realistic check on our results comes from Andreani & Franceschini (1995), who measured a complete sample of IRAS galaxies at 1300 μm (240 GHz). Their average flux ratio of 1300 μm over 100 μm is half that of the Galaxy, but one of their beam correction methods brings their ratio into agreement with the Milky Way. They find that the 60 μm emission of spiral galaxies receives enough contribution from a starburst dust component mostly absent in the Galaxy that including 60 μm fluxes in our fits may have caused a factor of 2 overestimate. Combined, these corrections give us a possible systematic overestimate of anisotropy by a factor of 4. If typical IR-bright galaxies have dust colder than the Milky Way, our results

could instead be an underestimate by a factor of a few, but this appears less likely. Our total systematic error is probably less than a factor of 3, which is consistent with our good agreement with previous results discussed in Section 3.

The recently obtained spectral knowledge of our Galaxy has enabled us to take into account the possible presence of Cold Dust. Our predicted level of temperature anisotropy makes the extragalactic infrared foreground dominant over the Galactic foregrounds of dust, free-free, and synchrotron for angular resolutions near $10'$ and frequencies above 100 GHz. Below 100 GHz, radio sources are expected to be the dominant extragalactic foreground. The extragalactic infrared foreground will not be significant in comparison to CMB anisotropies around 100 GHz but will be dominant above 500 GHz. Despite the likely presence of Cold Dust in infrared-bright galaxies, our results leave a window at intermediate frequencies for the measurement of CMB anisotropies without significant confusion from extragalactic infrared sources.

5.   Acknowledgments

REFERENCES

Andreani, P. & Franceschini, A. 1996, MNRAS, 283, 85

Banday, A.J. et al. 1996, ApJ, 468, L85

Beichman, C.A., & Helou, G. 1991, ApJ, 370, L1

Bennett, C.L. et al. 1992, ApJ, 396, L7

Block, D.L., et al. 1994, A&A, 288, 383

Chini, R., & Krugel, E. 1993, A&A, 279, 385

Chini, R., et al. 1995, A&A, 295, 317

Condon, J.J. & Broderick, J.J. 1991, AJ, 102, 1663

Crawford, T. et al. 1995, ApJ, in press, astro-ph/9511069

Devereux, N.A. & Young, J.S. 1992, AJ, 103, 1536

Eales, S.A., Wynn-William, C.G. & Duncan, W.D. 1989, ApJ, 339, 859

Fisher, K.B., et al. 1995, ApJS, 100, 69

Franceschini, A., & Andreani, P. 1995, ApJ, 440, L5

Franceschini, A., Toffolatti, L., Danese, L., & De Zotti, G. 1989, ApJ, 344, 35

Hauser, M.G. 1995, Proceedings of IAU Symposium 168, "Examining the Big Bang and Diffuse Background Radiations"

Kogut, A., et al. 1996, ApJ, 464, L5

Kogut, A., et al. 1994, ApJ, 433, 435

Mather, J.C., et al. 1994, ApJ, 420, 439

Neininger, N. & Guelin, M. 1996, Proceedings of Dust-Morphology Conference, Johannesburg, 22-26 January, (Kluwer Dordrecht), astro-ph/9603005

Odenwald, S., Newmark, J. & Smoot, G. 1995, ApJ, in press

Pearson, C. & Rowan-Robinson, M. 1996, MNRAS, 283, 174

Puget, J.-L., et al. 1996, A&A, 308, L5

Reach, W.T. et al. 1995, ApJ, 451, 188

Rowan-Robinson, M. 1992, MNRAS, 258, 787

Smoot, G.F. et al. 1992, ApJ, 396, L1

Smoot, G.F. et al. 1995, Astrophys. Lett., 32, 297

Tegmark, M. & Efstathiou, G. 1995, MNRAS, 281, 1297

Toffolatti, L. et al. 1995, Astrophys. Lett., 32, 125
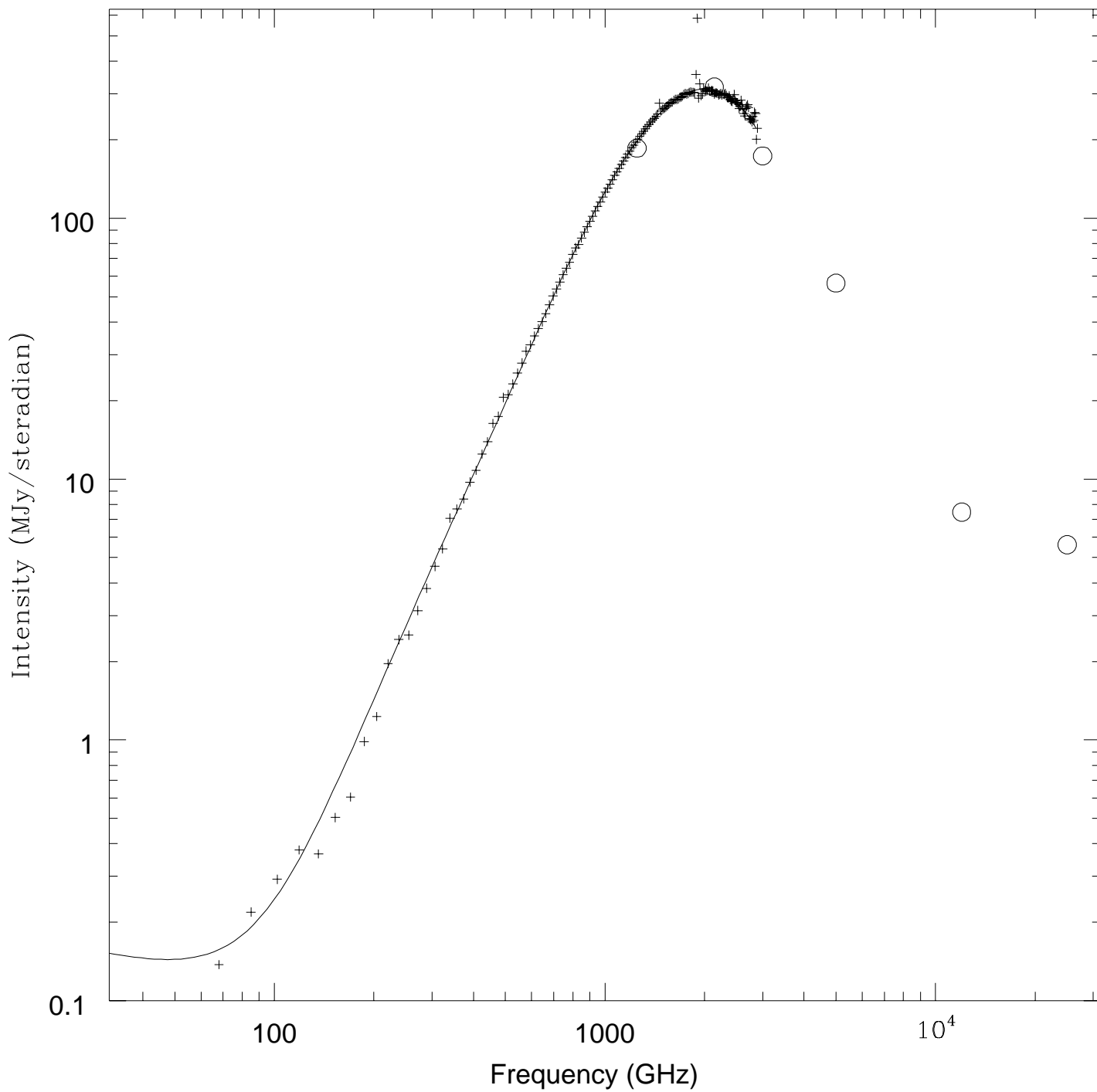
Wang, B. 1991, ApJ, 374, 465

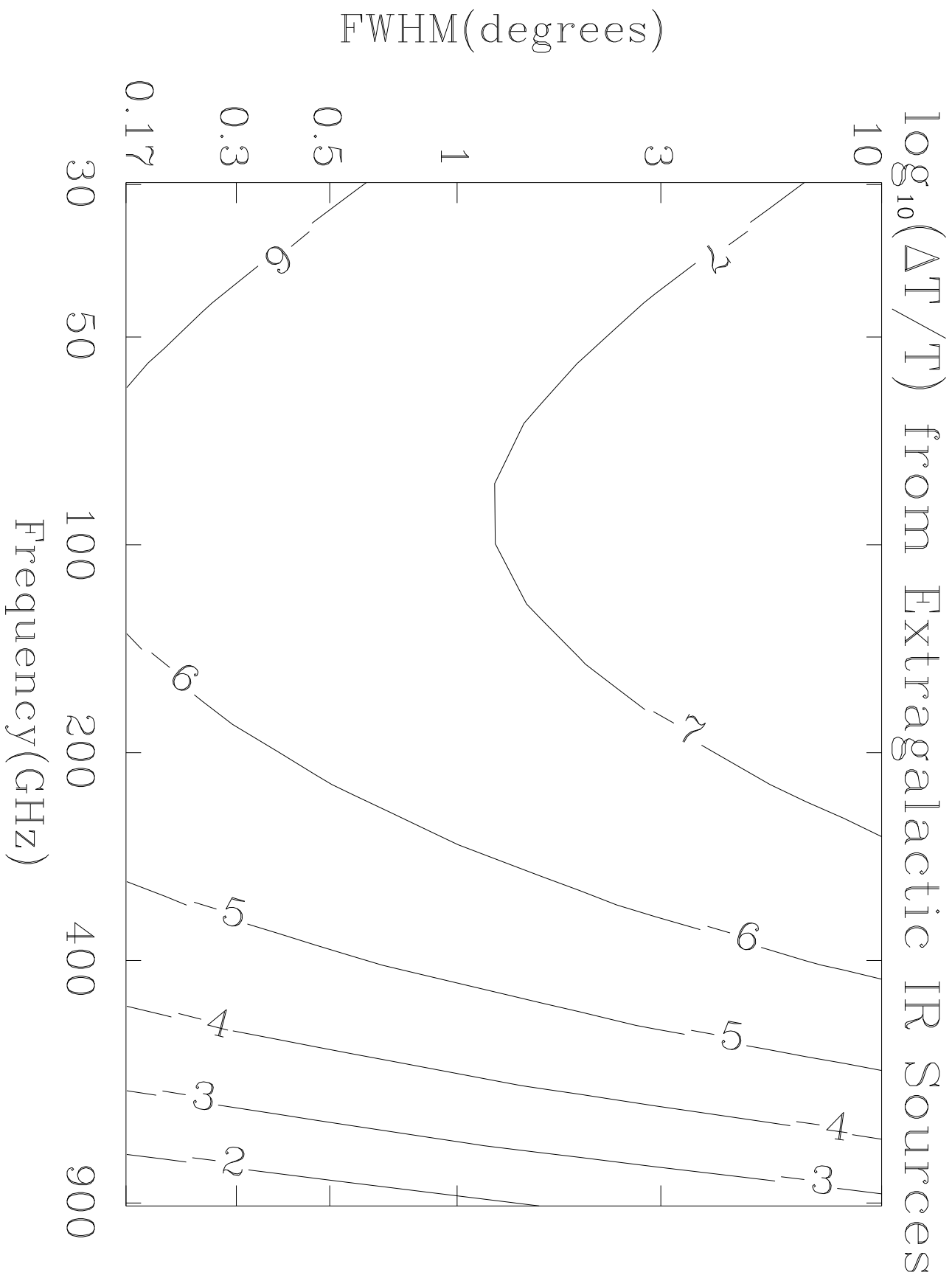Wright, E.L. et al. 1991, ApJ, 381, 200

Fig. 1.— The FIRAS Galactic Dust spectrum, including emission lines, is shown by + symbols. The smooth curve is a fit to this spectrum based upon a two-component dust model with synchrotron and free-free emission included using DMR results. With a ν^2 emissivity law assumed, the fit is Warm Dust at 19.4K and Cold Dust at 4.3K with an optical depth 12.1 times that of the Warm Dust. The FIRAS error bars are not shown because they are extremely small on this scale. The open circles are DIRBE integrated Galactic fluxes at 12, 25, 60, 100, 140, and 240 μm, normalized to the FIRAS measurements.

Fig. 2.— A log-log-log contour plot of equivalent thermodynamic temperature anisotropy due to extragalactic infrared sources as a function of frequency in GHz and angular resolution (FWHM) in degrees. The temperature anisotropy shown is $\log_{10} \frac{\Delta T}{T}$ where ΔT is the root mean square equivalent thermodynamic temperature generated by extragalactic infrared sources in Kelvin and T is the temperature (2.73K) of the CMB. The increase in anisotropy at low frequencies occurs because synchrotron and free-free emission are included in our template spectrum.

Fig. 3.— Log-log plot of $\frac{\Delta T}{T}$ versus frequency for instrument resolutions of 10′, 30′, 1°, and 10°, showing window where foreground confusion should be less than 10^{-6}. Solid lines are for no pixel subtraction. The dotted, dashed, and long-dashed lines show the results with pixels at a level of 5σ removed for resolutions of 10′,30′, and 1°, respectively. This 5σ subtraction makes no difference at any frequency for 10°.

Galactic Far-infrared Emission Spectrum

Confusion from Extragalactic Infrared Foreground Anisotropy